Analytical Chemistry
April 2019, Volume 91, Issue 9, Pages 6190-6199
https://doi.org/10.1021/acs.analchem.9b00849
https://archimer.ifremer.fr/doc/00489/60037/

More than 5% Ionization Efficiency by Cavity Source Thermal Ionization Mass Spectrometry for U Sub-ng Amounts.

Trinquier Anne [1, *], Maden Colin [1], Faure Anne-Laure [2], Hubert Amélie [2], Pointurier Fabien [2], Bourdon Bernard [3], Schönbächler Maria [1]

[1] ETH Zürich, Institute of Geochemistry and Petrology, Clausiusstrasse 25, CH-8092 Zürich, Switzerland
[2] CEA, DAM, DIF, 91297 Arpajon Cedex, France
[3] Laboratoire de Géologie de Lyon, ENS Lyon and UCBL, UMR 5276, CNRS, France

* Corresponding author : Anne Trinquier, email address : anne.trinquier@ifremer.fr

Abstract :

Numerous applications require the precise analysis of U isotope relative enrichment in sample amounts in the sub-nanogram to picogram range, among those are nuclear forensics, nuclear safeguards, environmental survey and geosciences. However, conven-tional thermal ionization mass spectrometry (TIMS) yields U combined ionization and transmission efficiencies (i.e ratio of ions detected to sample atoms loaded) less than 0.1 or 2% depending on the loading protocol, motivating the development of sources capable of enhancing ionization. The new prototype cavity source TIMS at ETH offers improvements from 4 to 15 times in com-bined ionization and transmission efficiency compared to conventional TIMS, yielding up to 5.6 % combined efficiency. Uranium isotope ratios have been determined on reference standards in the 100 pg range bound to ion-exchange or extraction resin beads. For natural U standards, n(235U)/n(238U) ratios are measured to relative external precisions of 0.5 to 1.0 % (2RSD, 2n<11, conven-tional source) or 5.6 % (2RSD, n=6, cavity source) and accuracies of 0.1 to 2.5% (conventional source) or 0.5 to 8.3% (cavity source), which would benefit further from in-run organic interference and peak tailing corrections.

Thermal ionization cavity sources were pioneered in the 1970's at radioactive beam facilities,[1-2] developed further in the 1990-2000's[3-5] and subsequently applied to TIMS instruments at Oak Ridge National Laboratory and the IAEA's Safeguard Analytical Laboratory,[6-7] as well as at the Northwest Institute of Nuclear Technology,[8] with the goal of analyzing the isotopic composition of actinides to identify the source of nuclear materials within the framework of nuclear safeguards.

The ionization efficiency of U liquid loads on Re filaments is limited to 0.01-0.1% without additives[7,8,9] and to 0.5-2% when adding Re powder and carbon over U bound to an ion-exchange resin bead[10] or using porous ion emitters.[11] To conduct the analysis of low U sample amounts or U minor isotopes to a high precision by TIMS, there is a need to compensate this less than 2 % ions detected per sample atoms loaded, by either enhancing ionization efficiency, or by improving the detection capability for small ion beams. The latter can be done in multiple collection mode using low noise-to-signal amplifier Faraday cups, optionally combined with simultaneous detection on one ion counter.[12-15] The present study focuses on increasing ionization efficiency.

The process of thermal ionization, also referred as surface ionization, involves ionization at the surface of a heated refractory metal, following the Saha-Langmuir equation[16]

$$\frac{N^+}{N^0} = A\, exp^{[e(\phi - I)/kT]} \quad (1)$$

where N^+ and N^o are, respectively, the number of single charged ions and neutral atoms leaving the surface of the filament per unit area per second, A is the ratio of statistical weights of the ionic and atomic ground states (A_U = 0.769), e is the charge of an electron (e = 1.602 x 10^{-19} C), ϕ is the work function of the metal surface (eV), I is the first ionization potential of the ionized element (eV), k is the Boltzmann constant (k = 1.381 x 10^{-23} $J.K^{-1}$) and T is the temperature of the metal surface (K).

Different strategies have been used to enhance the work function of a refractory metal surface, which leads to increased ionization efficiencies. Among them, graphitization induces the formation of a composite Re-C layer with a work function of 5.84 eV, which is 0.4 eV higher than for the recommended work function of a polycrystalline Re surface.[17-20] However, the elevated first ionization potential of U (6.19405 (6) eV),[19-20] is still high relative to the Re-C work function, calling for additional strategies to enhance ionization of U further. One of them is ionization in a cavity source.

In a cavity source, ionization is mainly induced by surface ionization at the cavity refractory metal surfaces[21] and the cavity acts as a furnace for both evaporation and ionization of the sample. However, within a cavity, the probability of ionization is enhanced compared to the single contact with the ionizing surface in conventional TIMS. With a cavity temperature < 2700 K, this results from the combination of multiple surface contacts of evaporated atoms within the confined volume of the

cavity, and electrical fields generated by the space charges of the ions and electrons within the cavity that help guide the ions towards the cavity orifice, thus reducing collisions with the walls of the cavity and recombination into neutral atoms.[22]

In the present study, we investigate the U ionization capability of our modified TIMS (Finnigan™ MAT262™) whose source has been replaced with a novel, in-house built cavity source prototype.[23] This complements a preliminary study where U_3O_8 particles were successfully ionized and intends at constraining quantitatively the ionization efficiency of well characterized amounts of U bound to single ion-exchange or extraction resin beads. We then compare the resulting ionization and transmission efficiencies of U samples in the sub-ng range, and the precisions and accuracies of their U isotope ratios, to the corresponding outcome from a conventional source TIMS (Thermo Electron™ TRITON™). In particular, we aim at producing repeatable ionization efficiencies as well as precise and accurate U isotope ratios for natural U samples. For the sake of consistency and clarity, in the following, we compared our results solely with manuscripts documenting *combined* ionization and transmission efficiencies.

Experimental section

The ETH cavity source prototype design has been previously described in detail[23] and only main features are summarized in the Supporting Information.

Loading methodology

Preparation of U resin bead batches

We followed the resin bead loading approach developed for conventional TIMS where U is bound to a single ion-exchange resin bead.[24] One extraction resin and several ion-exchange resins were tested: the transuranic Triskem™ TRU™ resin (100-150 µm wet bead size), the Bio-Rad™ AG 1-X8 anion resin (180-425 µm wet bead size) and the Bio-Rad AG 50W-X12 cation resin (53-106 µm wet bead size).

Resin beads were rinsed in Bio-Rad columns by eluting dilute HNO_3 (TRU), dilute HCl (AG 1-X8), or 6 M HCl (AG 50W-X12) and subsequently conditioned to 8 M HNO_3 (TRU), 11 M HCl (AG 1-X8) or 0.13 M HCl (AG 50W-X12). Beads were pipetted and sorted out with respect to size and shape using an Eppendorf™ syringe under a binocular microscope. Then, 50 beads of similar size were pipetted into 0.5 mL of ca. 20 ppb U solutions in 8 M HNO_3 (TRU), 11 M HCl (AG 1-X8), 0.13 M HCl (AG 50W-X12) and left to adsorb U for 48 h.

U amount per resin bead

The bound U was leached from several resin beads individually with 1% HNO_3 to determine the corresponding U amount per resin bead by ICPMS (Thermo Scientific™ Element XR™) by comparison with Elemental Scientific™ ICPMS natural U standards of known concentrations (hereafter referred to as U_{nat}). U concentration measurements were performed in low resolution mode, on sequences of 31 s analyses interspersed with 3 min wash and 110 s take-up times.

When present, linear instrumental drifts were corrected using ISOPLOT 4 (developed by Dr. Ludwig at the Berkeley Geochronology Center). The analytical repeatability for the U standards lay in the range of 0.5-5.0% (2RSD) depending on the analytical session. Dilution uncertainty associated with Eppendorf pipettes according to information provided by the constructor and the weighing uncertainty of gravimetric standards have been propagated.

With the exception of the cation resin, analyses were typically performed on 5 to 10 distinct resin beads for each resin batch (n duplicate analyses, $n \geq 5$), each duplicate being measured twice (2 replicates). The reported uncertainty is the standard deviation of the duplicates (n>1), or the standard deviation of the replicates in the case of the cationic resin bead (n=1). The results and corresponding U standards are reported in Table 1. The scatter on the resin bead duplicates is always larger than the combined uncertainty from dilution and analytical repeatability and the U amounts vary more within the TRU resin beads than with AG 1-X8 beads. Attributing the U amount scatter in resin beads to bead size distribution would imply that hand-picking was most efficient with the AG 1-X8 resin, which was then preferred as the project developed. In addition, the orange color of the AG 1-X8 is an asset for „handpicking“ under a binocular microscope.

Table 1. Uranium amounts in resin beads

Resin bead	U per resin bead (pg) (± 2RSD)					
	CRM 112A		U_{nat}		IRMM-187	U500
	Bead duplicates[1]	Solution[2]	Bead duplicates[1]	Solution[2]	Bead duplicates[1]	
TRU	159 (± 38 %) (n=10)	169 (± 3%)				
AG 1-X8	141 (± 10%) (n=5)		140 (± 15 %) (n=10)	148 (± 1%)	154 (± 22 %) (n=7)	89 (± 7%) (n=5)
AG 50W-X12			197 (± 3 %) (n=1)			

[1]measured on n individual resin beads [2]inferred from the measured difference in concentration between the resin batch solution before and after introduction of resin beads

U resin bead loading

Prior to loading, cavities machined in-house from H.Cross company™ 99.99% purity rhenium were outgassed for several days. All loading steps were carried out under a binocular microscope. One resin bead loaded with U was pipetted from a set of 50 resin beads in U solution and deposited on a parafilm™. Remains of U solution adhering to the resin bead were dried with a Kimwipe™ tissue to avoid that additional U from the solution biased the ionization efficiency estimates. The resin bead was then taken up in 0.1 µL of glucose (1:10 glucose:water content) using a Hamilton™ syringe and loaded onto the tip of the sample holder of a previously outgassed cavity (Figure SI-

1) or at the surface of a previously outgassed filament. Glucose acts as a glue that maintains the resin bead in position. Different loading protocols are reported in Table 2. AquaDag™ (C colloidal solution), Alpha Aesar™ Pt powder (325 mesh, 99.9 % purity) and H.Cross company™ Re powder (325 mesh 99.99% purity) colloidal solutions were prepared with glucose, unless otherwise specified. In the presence of carbon (from the resin beads or from additives: glucose, AquaDag), U is reduced to its metal form. Upon heating, carbon is dissolved in Re,[24] triggering rhenium carbide formation. As a result, Re-C surfaces enhance the work function compared with pure rhenium[17-18] and, thus, the ionization of U. In addition, adapting the Pt electroplating method[27] to increase the work function of the ionizing surface further, Pt powder was added as a colloidal suspension in glucose on top of the resin bead. The additives were loaded in various sequences, depending on the protocol: (i) AquaDag + TRU resin (ii) TRU resin + Re (iii) TRU resin + Re + AquaDag (iv) Anion resin + AquaDag (v) Pt + anion resin (vi) Anion resin + AquaDag + Pt (vii) AquaDag + Pt + cation resin.

For loading samples onto the filament with conventional source TIMS, a 0.7 A current was passed through the filament during resin bead loading, and afterwards slowly ramped to 1 A for a few seconds to dry the additives reported in Table 2. To avoid arcing and because elevated filament running temperatures (> 2000 K) induced Re platting of double filament holder glass beads, only single Re filaments were used, for which the ionization surface lies orthogonal to the glass beads.

With the cavity source TIMS, the sample holder of a previously sample loaded cavity was placed on a hotplate at 323 K for a few minutes to dry the additives (reported in Table 2). The resin bead was always loaded prior to coating with additives, in a sequence: resin bead, AquaDag, Pt powder.

The cavities or filaments were then loaded in the vacuum chambers of the corresponding instruments.

Table 2. Loading protocols for U resin beads

Loading protocols					Efficiency (%) ± 2 SD		Median T (K)[4]	
Resin	Solutions and colloidal solutions[1]				Source		Source	
	Glucose	AquaDag[2]	Re	Pt[2]	Conventional	Cavity	Conventional	Cavity[5]
TRU - CRM 112A	0.1 µL				0.24 ± 0.08 (n=11)	3.57 ± 1.53 (n=2)	2053	≥ 2680
	0.1 µL	0.1 µL			0.15 ± 0.09 (n=3)		2003	
	0.1 µL		(0.1-0.3 µL)[3]		0.05 ± 0.02 (n=5)			
	0.1 µL	0.1 µL	(0.1-0.3 µL)[2]		0.08 ± 0.00 (n=2)		2108	
Anion resin AG 1-X8 - U_{nat}	0.1 µL				0.37 ± 0.09 (n=3)	4.90 ± 1.57 (n=3)	2083	
	0.1 µL	0.1 µL			0.33 ± 0.11 (n=6)	4.54 ± 1.53 (n=2)	2103	
	0.1 µL			0.1-0.3 µL	0.60 (n=1)		2133	
	0.1 µL	0.1 µL		0.1-0.3 µL	0.61 ± 0.34 (n=5)	2.57 ± 0.13 (n=2)	2163	
Cation resin AG 50W-X12 - U_{nat}	0.1 µL	0.1 µL		0.1-0.3 µL	0.15 (n=1)		2153	

[1] When loaded over resin beads, Pt and Re solutions were added until the resin bead was completely coated, causing the volumes to vary from 0.1 to 0.3 µL for the TRITON loads. This might have led to a slighty higher release of U in glucose during loading of these protocols for conventional source than for cavity source. For the cavity loading, the resin enclosed at the bottom of the conic depression of the sample holder was readily coated with 0.1 µL of colloidal solution. [2] suspension in glucose [3] suspension in ethanol [4] median of filament temperatures at the time when half of the ions have been collected [5] estimation from the melting point of Ir (see text for details).

Conditioning

Outgassing of the source and samples

Conventional TIMS source

Prior to analysis, slow ramping of the filaments was performed at a rate ≤ 50 mA/min up to 2 A for all protocols and up to 4.5 A for the Pt coating protocols, after which the samples were let to cool for several minutes before resuming heating and focusing at a pressure of about 10^{-7} mbar, or lower. The pressure in the source housing during focusing and analysis was typically between 0.9 and 2.6 $\times 10^{-7}$ mbar, with the exception of 3 analyses whose pressures varied from 2.4 to 5.1 $\times 10^{-7}$ mbar. The median pressure of all analyses was 1.4 $\times 10^{-7}$ mbar.

Cavity source

Slow cavity heating preceded analysis to (i) avoid resin bead violent decomposition and U loss, (ii) minimize the pressure increase in the source (and the flight tube) and (iii) avoid interrupting analyses due to arcing at source pressures in excess of 10^{-6} mbar. A first ramping to 100 W heating power at 2.5 W/min ($P \leq 4\times10^{-7}$ mbar) was followed by ramping to 200 W at 5 W/min ($P \leq 6\times10^{-7}$ mbar) and cooling until the pressure in the

source returned to the stand-by pressure ≤ 10^{-7} mbar. The entire resin bead conditioning and cooling step took 7 hours.

Pressure during focusing and analysis in the cavity source was between 1 and 15×10^{-7} mbar. At the upper limit, which was reached after about 1 hour of operation, the analyses were stopped and the filament and cavity let to cool. The analytical session was resumed when the pressure reached the stand-by regime of 10^{-7} mbar.

Heating and focusing of the U samples for analysis

Conventional TIMS source

The heating of the filament was monitored with the two-channel digital pyrometer installed on the TRITON instrument. Source tuning consisted in adjusting the source lens stack potentials for maximum signal prior to analysis. This operation was also repeated automatically during analysis.

Cavity source

The repeller shield voltage focuses the electron bombardment (EB) beam onto the sample holder - cavity assembly. It is tuned after each EB filament exchange (4 times in 19 months) by monitoring the temperature distribution with a pyrometer such as to maximize the temperature at the surface of the cavity tube, and have the temperature of the cavity (ionization) exceed that of the sample holder (evaporation). Due to it being a single-channel pyrometer and its view port getting coated with material sublimated from the cavity, absolute temperature readings were considered unreliable and the pyrometer was solely used to monitor relative temperature differences of the cavity. Further repeller voltage adjustments were repeated consequently to EB filament aging and thinning. During sample heating and between consecutive analyses, tuning mainly relied on adjusting manually the x-y-position of the cavity assembly relative to the source lens stack with the x-y-z-stage. This partly compensated for signal instability and optimized the ion extraction efficiency.

To a lesser extent, slight adjustments of the tuning of the repeller shield voltage could prove useful during heating.

After an initial optimization at the beginning of this project, it proved unnecessary to re-adjust the cavity source lens stack voltages.

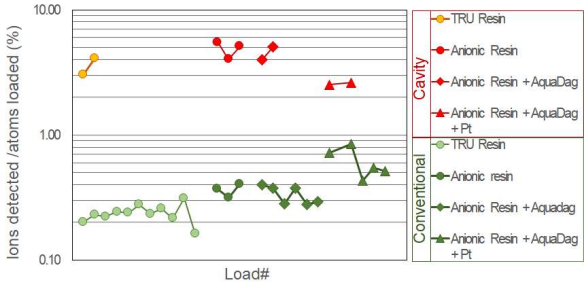

Figure 1. Comparison of the ionization and transmission efficiency for ca. 150 pg U loads on individual ion-exchange or extraction resin beads, between conventional source and cavity source TIMS, using identical loading protocols (Table 2). Additional protocols tested by conventional TIMS are reported in Table 2. The enhancement in ionization and transmission efficiency is a factor of 4 for the Pt-protocol and more than ten-fold, otherwise (see text and Table 2 for details).

Ionization and transmission efficiency determination

Combined ionization and transmission efficiencies were determined by running standards of known U amounts (CRM 112 A with the TRU resin and U_{nat} with the anion and cation resins, Table 1) to complete exhaustion, monitoring ^{238}U beams with low mass resolution settings (corresponding to a 0.8 mm wide source slit on the cavity source), and calculating the ratio of detected ions to loaded atoms (Table 1 and Figure 1).

U isotope ratio analysis

Choice of source slit width

For cavity source TIMS, using a 0.8mm wide source slit degrades the mass spectrum peak shapes.[23] Instead, for a better plateau on the peaks for analysis, U isotope ratio measurements were carried out with a 0.3 mm wide source slit leading to an about 2-times increased mass resolving power, with the side effect of losing signal intensity by a factor 1.67 compared to a 0.8 mm wide slit.

Baselines

During TIMS with a conventional source, thirty second electronic baselines were measured with a defocussed ion beam every 6 min, whereas, with cavity source TIMS, baselines consisted of on-peak zero (OPZ) electronic background measurements of the Faraday cups on masses where no signal was expected (Pu isotopes) or whenever the signal remained below the Faraday cup detection limit (mass 237.05 u) (see below protocols 2 and 3, Table 3).

Data reduction

The different U measurement strategies are summarized in Table 3.

Measured U isotope ratio means are calculated as the averages of block means weighted with the corresponding block uncertainties.

By conventional source TIMS, resin beads were measured only once to complete exhaustion, following a Total Evaporation protocol and analyses consisted of several blocks of 63 to 126 s integrations each on $^{234,235,238}U$ masses (Table 3).

By cavity source TIMS, a resin bead was measured over several heating sessions over one day or more, and each heating session yielded one measurement that combined several blocks interspersed by focusing and heating intervals. A block was defined as the analysis of 10 times 8s integrations on $^{234,235,238}U$ masses (Table 3). Signal drift linear temporal interpolation corrections were applied on a per integration basis. For the TRU resin bead, heating sessions covered several days and each of the 4 replicates correspond to the mean of heating sessions covering one day (Tables S1 and S2).

Following previous approaches,[12,15] only ratios corresponding to ^{238}U > 1mV (I > 0.01 pA) were included in the data reduction.

Uncertainty assessment

Faraday cup detection system

On the conventional source instrument, Faraday cup amplifiers with 10^{11} Ω feedback resistors have been checked for baseline stability and those with less than 20 μV noise (1SD, 4 s integration time) were selected for analysis. Amplifier gain stability was within 10 ppm (1SD). OPZ baselines of cavity source analyses were corrected for on a per integration basis (Protocols 2 and 3, Table 3). The associated uncertainty is expected to be reflected in the run analytical precision.

The cross-calibration of Faraday cups can be assessed during analysis by measuring ^{238}U on different Faraday cups (Protocol 2, Table 3). Within analytical uncertainty, Faraday cup factors were not resolved for the cups monitoring ^{235}U and ^{238}U in protocols 2 and 3 and were therefore neglected. In any case, any significant drift or bias in the cup factors should be represented in the final run analytical precision.

Table 3. Protocols for U isotope analysis

Conventional TIMS Source						
Protocol-1	SEM	FAR2	FAR3	FAR4	Integration time (s)	Measurements
Magnet setting-1	^{234}U	^{235}U	237.05 u	^{238}U	8.4	$^{234}U_{SEM}/^{238}U_{FAR4}$
Magnet setting-2	237.05 u	^{238}U			4.2	$237.05_{SEM}/^{238}U_{FAR2}$ (abundance at mass 237)
Magnet setting-3	^{235}U	^{236}U	^{238}U		4.2	$^{235}U_{SEM}/^{238}U_{FAR3}$
Cavity Source						
Protocol-2	FAR1	FAR2	FAR3		Integration time (s)	Measurements
Magnet setting-1	237.05 u	^{238}U	^{241}Pu		8	OPZ (237.05_{FAR1}, $^{239}Pu_{FAR2}$, $^{241,242}Pu_{FAR3}$)
Magnet setting-2	^{238}U	^{239}Pu	^{242}Pu		8	Cup factors and peak overlap ($^{238}U_{FAR1}$, $^{238}U_{FAR2}$, $^{238}U_{FAR3}$)
	SEM	FAR2	FAR3			$^{234}U_{SEM}/^{238}U_{FAR3}$, $^{235}U_{FAR2}/^{238}U_{FAR3}$
Magnet setting-3	^{234}U	^{235}U	^{238}U		8	
Protocol-3	SEM	FAR2	FAR3			Measurements
Magnet setting-1	^{234}U	^{235}U	^{238}U		8	OPZ ($^{239}Pu_{FAR2}$, $^{239,242}Pu_{FAR3}$)
Magnet setting-2	^{235}U	^{236}U	^{239}Pu		8	Yield and SEM/FAR3 peak overlap ($^{238}U_{SEM}/^{238}U_{FAR3}$)
Magnet setting-3	^{238}U	^{239}Pu	^{242}Pu		8	Yield ($^{235}U_{SEM}/^{235}U_{FAR2}$)

Relative yield between SEM and Faraday cups

On both instruments, the dark noise on the secondary electron multiplier (SEM) was less than 10 cpm.

By conventional source TIMS, the yield between the SEM and Faraday cups (typically 95-96%) was assessed by peak hopping measurement of a stable ^{238}U ion beam on the SEM and a Faraday cup prior to analysis. The precision of the yield estimation was less than the certified drift of a SEM (0.2%/h 1RSD at 300 kcps, constructor information). No uncertainty was propagated as the SEM drift variability is already represented in the repeatability of $^{234}U/^{238}U$ and $^{235}U/^{238}U$ ratios.

By cavity source TIMS, for $^{235,238}U$ ion beams < 10 mV ($I^{235}U$ and $I^{238}U$ <0.1 pA), the SEM-to-Faraday cup yield was assessed during analysis using ^{238}U ion beams measured alternatively on the SEM and a Faraday cup, and corrected on a per integration basis (Protocol 3, magnet settings-1 to 3, Table 3). For ^{238}U > 10 mV and ^{235}U < 10 mV, the applied yield was the weighted mean of the yield assessed using ^{235}U ion beams (Protocol 3 limited to magnet settings 1 and 2) and the ^{238}U-yield(s) measured in the previous analyses. In this case, the yield correction was applied to the mean values of $^{234,235}U/^{238}U$ ratios of each analysis, with associated yield uncertainty propagation.

For $^{235,238}U$ ion beams > 10 mV (Protocol 2), the SEM-to-Faraday cup yield correction on the mean values of $n(^{234}U)/n(^{238}U)$ ratios was performed using the ^{238}U-yield measured in the previous analyses, with associated yield uncertainty propagation. The median yield was 102 ± 0.6% with variations from session to session between 101 and 103 % and analytical uncertainties between 0.2 and 2.3 %.

Background on $^{234}U/^{238}U$

The most accurate and reproducible protocol to correct for U abundance sensitivity on ^{234}U would consist in interpolating between the background levels measured at ^{234}U half-masses within the same analyses, using Faraday cups connected to high-resistance amplifiers or ion counting detection.[12,15] However, in this preliminary study, the priority was given to the determination of U ionization efficiency and of the precision on $n(^{235}U)/n(^{238}U)$ ratios. Consequently, with the intent to maximize the measuring time and, thus the counting statistics, on $n(^{235}U)/n(^{238}U)$ ratios, ^{234}U half-masses were not monitored. Instead, an alternative and crude approach has been pursued by deriving ^{234}U background from the monitoring of mass 237.05 u measured within the same blocks and described thereafter (Figure 2).

Results and discussion

U ionization and transmission efficiency

The comparison of combined ionization and transmission efficiency obtained with cavity source TIMS and conventional source TIMS is summarized in Table 2 and Figure 1. The 2SD uncertainty in efficiency is consistent with, or largely resulting from, the heterogeneous distribution of U contents from bead to bead (Table 1). Although Pt coating protocols are the most efficient with conventional source TIMS with an ionization and transmission efficiency of up to 0.6 %, Pt-free loading protocols yield the largest efficiency improvements with factors ranging from 13 to 15, for the anionic resin and the TRU resin, respectively. In the case of the Pt-coated protocol, the enhancement in the overall efficiency using the cavity is about a factor of 4, which is 3 – 4 times lower than for the Pt-free loading methods. Within uncertainty, AquaDag addition does not affect much the ionization and transmission efficiency, potentially implying that U samples are already fully reduced by the C present in the resin and glucose and that the work function of Re-C surfaces is already at its maximum. The best combined ionization and transmission efficiencies for 100-200 pg U loads obtained with our Re cavity design are reached with the anion resin and range from 4.00 to 5.56 %. Statistically indistinguishable, two protocols yield 4.90 % efficiency (AG 1-X8, n=3) and 4.54 % efficiency (AG 1-X8 - AquaDag, n=2), in line with the mean efficiency of 5.8 % (n=17) reported by a different group based on the analysis of 100-500 pg U loads,[6] although we used different resin bead loading protocols, ion source lens stack, cavity design and likely lower operational temperature regimes in the present study. Notably, our efficiencies are reproducible to bet-

ter than 30% (2RSD). Considering that about a third of the scatter in the estimation of the efficiencies can be ascribed to U variable amounts in resin beads (Table 1), our efficiencies appear more repeatable by one to two orders of magnitude compared to previous studies.[6] Lastly, it is worth mentioning that combined efficiency first order estimates (3 – 19 %) for uranium oxide particles using the same ion source[23] lie within the more precise, reproducible and accurate range of the present work.

Unraveling the efficiency enhancement between conventional and cavity source TIMS

Depending on the resin bead loading protocol, the ionization and transmission efficiency is increased by factors 4 to 15 between the conventional source and the cavity source, whereas ionization temperatures increase by about 600 K (Table 2). However, assuming identical work functions on both instruments, the Saha-Langmuir equation (1) predicts that the temperatures should rise by about 2660 K, using AG 1-X8 Pt-free protocols. Therefore, the observed efficiency enhancement cannot exclusively result from single-surface-contact thermal ionization and illustrates a gain of about one order of magnitude in ionization efficiency provided by the geometry of the cavity source.

In the Supporting Information, we show that, to the first order, combined Sofie and SIMION simulations[22,23] can reproduce our experimental results.

Platinum-C catalyst behavior

Pt-coated sample loading protocols on the conventional source are run at temperatures in excess of 30 to 50 K compared to those of Pt-free protocols (Table 2) but provide a factor 1.7 better ionization efficiency than Pt-free protocols. However, based on this temperature increase alone, the Saha-Langmuir equation (1) would predict a gain in ionization efficiency of merely about 15%. Another effect must come into play. With the conventional source, Pt-C coating induced enhancement capability for U ionization seems to depend on the temperature regime. Pt-C act as a poor catalyst in the optimal temperature regime of Pt-free protocols, as inferred from lower ion beam intensities, unpredictable U isotope fractionation and unstable U signals. In contrast, at temperatures 50 K above optimal for Pt-free protocols (Table 2), Pt-C acts as an activator. Such different catalyst regimes have been reported for Pt surfaces coated with C, with varying work functions in the eV range associated with the crystalline evolution of C with temperature.[28] With unpredictable U isotope fractionation and poorer ionization efficiency than Pt-free protocols, cavity source Pt-coated protocols seem to suffer from similar effects. However, given that the cavity is operated at temperatures 500 to 600 K higher than for conventional filament TIMS, the physico-chemical processes involved require further investigation.

Comparison with MC-ICPMS and LG-SIMS ionization efficiencies

More than 5 % combined ionization and transmission efficiency can be obtained for U loads in the 100 pg range with our cavity source design. This represents a 2 to 3-fold improvement compared to multiple collection inductively coupled plasma mass spectrometry (MC-ICPMS). The best efficiency obtained for U in the sub-ng range with a Thermo Scientific™ NEPTUNE *Plus*™ MC-ICPMS is approximately 1.5-2.5%.[29] Meanwhile, assuming that the cavity source ionization efficiency of U pg loads is greater than or equal to that of U 100 pg loads, this would represent a 3-5-fold improvement compared to large geometry secondary ion mass spectrometry (LG-SIMS). Based on experimental measurements on U oxide particles in the pg range, Cameca 1270™ LG-SIMS provides 1.2 and up to 1.7% efficiency depending on the sputtering beam, for converting U atoms into detected ions.[30-31] Notably, with all three settings (cavity source TIMS, MC-ICPMS and LG-SIMS), special attention has to be paid to limit background effects. However, MC-ICPMS and SIMS analyses also require $^{235}U^{1}H$ uranium hydride interference correction on the measured ^{236}U, thus degrading their ^{236}U detection limits.[29-31]

Ionized Species

Uranium oxides

U_{oxide} and U_{metal} ion species could compete in the vapour phase and limit the ionization efficiency of U_{metal}.[13,27] Uranium oxide-to-metal ratios were monitored at $^{238}U^{16}O$ and $^{238}U^{16}O_2$ masses. With the conventional TIMS source, U oxide species are detectable and appear more elevated in filament blanks, than after addition of C-rich resin beads and additives, supporting efficient reduction by C in the latter case. In addition, U_{oxide}/U_{metal} ratios diminish with increasing temperature and are less than 0.3% when analyses are started.

In contrast, there are no detectable amounts of U_{oxides} with the cavity source within the operational ionization temperature regime, potentially owing to efficient outgassing prior to analysis, a prolonged reduction of U by the C provided by the resin beads and to more elevated ionization temperatures than with conventional TIMS (Table 2).

K impurities and potential K-cluster interferences

Among detected impurities, K signals are of potential concern because K-clusters could affect U minor isotope backgrounds (i.e. $^{39}K_6$ interferes at mass 234 u). K-clusters of K_x species with x ranging from 2 to 8 have previously been characterized[32] and K_6 species have been observed on ^{236}U (ref. 12) and ^{234}U by B. Bourdon by conventional TIMS. The resin beads do not contribute significantly to the K budget and the contamination seems to mainly originate in the source components, Re cavity and Re filaments. With the conventional TIMS source, K largely originate from source outgassing as evidenced by an increase of the detected amounts after halogen lamp degassing of the source. With the cavity source, at U ionization temperatures, ^{39}K contributions are minimum and less than with the conventional source.

Correlated $n(^{234}U)/n(^{238}U)$ and $237.05/n(^{238}U)$ variations

For conventional source TIMS analyses, the $n(^{234}U)/n(^{238}U)$ ratios of CRM 112A and U_{nat} standards using TRU, anion, and cation resin bead protocols correlate with the corresponding abundance sensitivity at mass 237.05 u measured within the same blocks (Figure 2) as expected from peak tailing of major U isotopes onto minor ^{234}U. However, a crude and conservative estimation of the peak tailing contributions support that elevated $n(^{234}U)/n(^{238}U)$ ratios relative to the corresponding CRM 112A certified reference[12] cannot be solely accounted for by peak tailing from $^{235,238}U$ isotopes onto ^{234}U. If the most elevated $237/n(^{238}U)$ ratio of about 2.5×10^{-5} (Figure 2) was interpreted as a peak tailing contribution from ^{238}U, this would translate into an increase of less than 6.2×10^{-6} in the corresponding $n(^{234}U)/n(^{235}U)$ ratio from the tailing of ^{238}U. One could anticipate an additional increase of ca. 25 ppm in the $n(^{234}U)/n(^{235}U)$ ratio from the tailing of ^{235}U, implying a subsequent excess in the ratio $n(^{234}U)/n(^{238}U)$ of $(7.3\times10^{-3}) \times (2.5\times10^{-5}) = 1.8\times10^{-7}$. Therefore, the maximum peak tailing from $^{235,238}U$ isotopes onto

^{234}U would be less than 6.4×10^{-6}, which is a third of the observed increase of ca. 2.0×10^{-5} (Figure 2). Such peak tailing would correspond to a *maximum* correlation slope of about 0.26 in Figure 2. The same line of reasoning applied to IRMM-187 would induce a *maximum* regression slope of 0.30 between n(^{234}U)/n(^{238}U) and 237/n(^{238}U), in line with the measured value of 0.174 (45) previously assessed by the analysis of IRMM-187.[26] Instead, the inferred slope of 0.73 (21) in Figure 2 is significantly more elevated than derived from these conservative estimates.

As the correlated excesses in n(^{234}U)/n(^{238}U) and 237.05/n(^{238}U) ratios cannot derive from K-clusters, they most likely result from the presence of organic interferences, in line with the previous observation of organic species in the range 230 to 238 u associated with the analysis of U particles loaded with collodion by the CEA contributors of this study. The highest excesses in ^{234}U relative to CRM 112A (ref. 12) are typically observed at the beginning of analyses of U bound to anionic resin (AG 1-X8) beads, (i) without additives other than glucose, (ii) with AquaDag or (iii) with AquaDag and Pt.

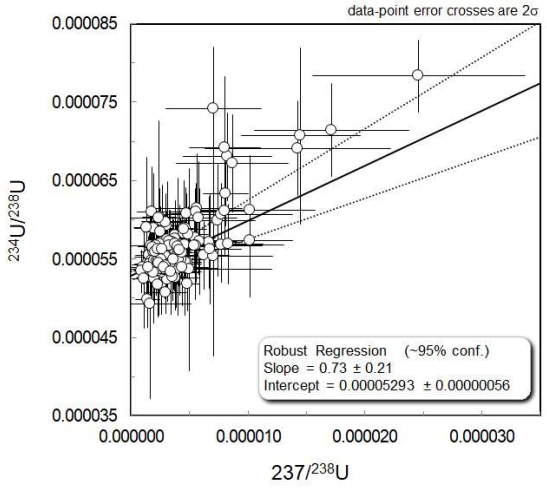

Figure 2. Correlation between the signal measured at mass 237 u and the measured ^{234}U/^{238}U ratios for all loading protocols, by conventional source TIMS, which cannot be solely ascribed to a peak tailing contribution from major U isotopes to the minor ^{234}U isotope and requires the presence of interfering species of correlated abundances at masses 234 and 237 u. The intercept of the regression (in the absence of peak tailing and interference contributions) is in agreement with the certified CRM 112A reference value,[12] within uncertainty (see text for details).

No trend could be observed between excess ^{234}U and the pressure monitored in the source housing. However, there are trends between ^{234}U excesses and the temperature of the filament in anionic (AG 1-X8) and cationic (AG 50W-X12) resin bead loads, with excesses diminishing with ramping temperatures, pointing towards organics burning off. In the absence of ^{234}U half-mass in-situ monitoring, a crude correction for peak tailing and organic background contributions to n(^{234}U)/n(^{238}U) ratios is applied, using the linear regression of n(^{234}U)/n(^{238}U) and 237.05/n(^{238}U) covariations (inferred from ISOPLOT 4 developed by Dr. Ludwig at the Berkeley Gechronology Center). For the anion and cation resin beads, the reported n(^{234}U)/n(^{238}U) ratios are previously corrected for mass bias on a per integration basis, using the exponential law and the n(^{235}U)/n(^{238}U) ratios measured within the same analyses (Table S2 and Figure 2). Notably, the intercept of the resulting regression (237.05/^{238}U = 0) yields the certified CRM 112A n(^{234}U)/n(^{238}U) ratio, within uncertainty. Any bias to the regression slope induced by applying an exaggerate U fractionation correction to measured n(^{234}U)/n(^{238}U) ratios, which include peak tailing and interference contributions that do not require mass bias correction, remains negligible with respect to the uncertainty on the slope derived from ISOPLOT.

Subsequently, n(^{234}U)/n(^{238}U) ratios are corrected for peak tailing and background using the regression slope on a per block basis. The uncertainties on the measured 237.05/^{238}U ratios and on the regression slope are propagated in the n(^{234}U)/n(^{238}U) ratio uncertainties.

By cavity source TIMS, no peak tailing correction was performed because neither half-masses of ^{234}U nor mass 237.05 u were measured on a SEM to maintain the analysis time to about 5 min, in order to be able to focus the signal intensity with the x-y-z stage at short time intervals.

Pt coating specific impurities

Sr and Rb impurities are present in the Pt loads. With the conventional source, whenever the samples are not heated to temperatures about 30-50 K higher than with the Pt-free protocols (Table 2), the U ion beams are unstable and the U data scatter in unpredictable ways (not reported). Instability and unpredictable isotope fractionations are also visible with the cavity source (not reported). This could be associated with the presence of molecular interferences whose abundance decrease with increased heating. However, by conventional source, whenever heated to temperatures in excess of 50 K compared to those of Pt-free protocols, Pt protocols associated with the anionic resin AG 1-X8 yield the best ionization and transmission efficiencies for U and the repeatability of U data is in line with those of other protocols (Tables S1 and S2).

U blanks

The anion resin U blanks measured on the Element XR yielded 0.050 ± 0.016 pg (2RSD, n=5) and are, as such, negligible. The loading blank (filament, anionic resin, additives and handling) has been monitored on several cavities with a 0.3 mm wide source slit at measurement conditions (i.e. between 300 and 400 W heating power). This yielded ^{238}U ion beams in the range of 5-10 kcps, representing a tenth or less of the Mcps ^{238}U ion beams measured for 100-150 pg U loads. The loading blank has been measured to be of natural isotopic composition, and the amount thereof has been assessed by the analysis of the enriched standard U500. Raw ^{234,235}U/^{238}U isotope ratios of U500 without mass bias nor peak tailing correction indicated a maximum U_{nat} contribution of 1.2% of the overall U load, thus corresponding to a maximum 1 pg natural U overall blank, which required acceptable corrections for 100 pg U loads (Tables S1 and S2). In this study, no blank correction has been performed for natural U standards. A blank correction has been carried out on the IRMM-187 enriched certified standard as reported in Tables S1 and S2.

U isotope ratios

Precision and accuracy of cavity sources are verified for the first time on natural n(^{235}U)/n(^{238}U) ratios.

Expanded uncertainties

The weighted means and expanded uncertainties of n(^{235}U)/n(^{238}U), peak tailing and interference corrected

$n(^{234}U)/n(^{238}U)$ (conventional source) and non-peak tailing nor interference corrected $n(^{234}U)/n(^{238}U)$ (cavity source), are reported for each analytical protocol in Tables S1 and S2.

Conventional TIMS source

For $n(^{235}U)/n(^{238}U)$ ratios, the expanded uncertainties correspond solely to the measurement uncertainty. The mean expanded uncertainties are typically between 0.1 and 0.3%, and amount to up to 0.6% for the TRU resin protocol with AquaDag- Re coating, in line with lower counting statistics associated with the lowest ionization and transmission efficiency of all protocols (~ 0.08%, Table 2). For $n(^{234}U)/n(^{238}U)$ ratios corrected for peak tailing and interferences, the expanded uncertainty combines the weighted precision on $n(^{234}U)/n(^{238}U)$, the weighted precision on the measured $237.05/n(^{238}U)$ and the uncertainty on the regression slope (Figure 2). The mean expanded uncertainties are dominated by the weighted precision on $n(^{234}U)/n(^{238}U)$ and are between 1.6 and 2.4 % (4.8 % for the TRU - AquaDag - Re protocol) after peak tailing and interference correction for all U loads, and mass bias correction for U_{nat} loads. Overall, the expanded uncertainty is of the order of the combined noise originating from counting statistics (Shot Noise), Johnson-Nyquist Faraday cup amplifier noise and SEM noise (typically 2 to 27 permil noise on $^{235}U/^{238}U$ integrations of 8.4s).

Cavity source

The expanded uncertainty combines the weighted precision and the yield correction uncertainty, when applicable.

The average $n(^{235}U)/n(^{238}U)$ in-run expanded uncertainty is between 0.5 and 0.7 % for natural U standards (CRM 112A and U_{nat}), IRMM-187 and U500 (Table S1). The average $n(^{234}U)/n(^{238}U)$ in-run expanded uncertainty is between 1.1 and 2.7% for natural U standards (CRM 112A and U_{nat}), 0.9% for IRMM-187 and 0.4% for U500 (Table S2). The better expanded uncertainty of ^{234}U enriched IRMM-187 and U500, compared to natural U standards can be accounted for by lower peak tailing and organic interference contributions, which can fluctuate during analysis, as observed for the conventional source. However, the same as for natural U standards, the expanded uncertainties of IRMM-187 and U500 exceed the uncertainty associated with the counting statistics and the detector noise alone by one order of magnitude. The measured-noise-to-theoretical-noise ratio for $n(^{235}U)/n(^{238}U)$ integrations of 8 s ranges from 7 to 39 with a theoretical relative noise between 0.4 and 11.3 permil, and a measured relative noise between 3.3 and 70.4 permil. Therefore, it can be inferred that a large contribution to the expanded uncertainties arises from signal fluctuations (up to 30%), which could be caused by thermal expansion of the EB filament during heating.

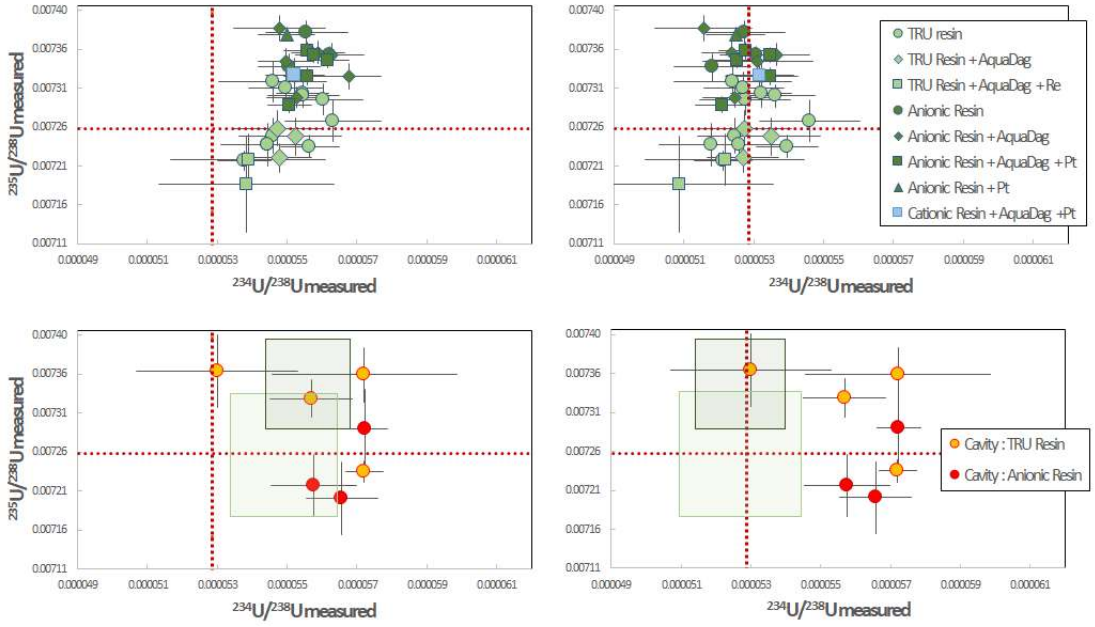

Figure 3. Uranium isotope ratios for natural U standards in this study. Top: conventional source TIMS U isotope ratios measured in this study. Top left: measured. Top right: after peak tailing and background correction (all resins) and internal mass bias correction (anionic and cationic resins) on $^{234}U/^{238}U$ measured ratios. Bottom: cavity source measured U isotope ratios plotted against conventional source U data represented as 2SD green boxes (left: without correction; right: with mass bias and peak tailing and background correction). Uncorrected cavity source data are consistent with conventional source data uncorrected for peak-tailing and background (bottom left). Red dotted lines correspond to reference values[12] (see text for details). Error bars are expanded uncertainties.

External precision

The external precision or repeatability is reported as the standard deviation of the replicate (cavity source) or duplicate (conventional source) measurements of one standard (Tables S1 and S2).

Conventional TIMS source

For $n(^{235}U)/n(^{238}U)$ ratios, the repeatability is of the same order or larger than the mean of in-run expanded uncertainties (0.5 to 1.0 %, depending on the loading protocol, Table S1). For $n(^{234}U)/n(^{238}U)$ ratios, the repeatability is often worse than the in-run expanded uncertainty and is improved after peak tailing and organic interference correction (1.7 to 3.6 %, depending on the loading protocol, Table S2).

Cavity source

For the TRU resin protocols, the repeatability is larger than the in-run expanded uncertainty, amounting to 2.0 % for $n(^{235}U)/n(^{238}U)$ and 5.6% for $n(^{234}U)/n(^{238}U)$, in the absence of peak tailing and organic interference correction (Tables S1 and S2).

Accuracy

NBL Certified Reference Materials (CRM) 112A and U500, and IRMM-187 were used to assess the accuracy of isotope ratio analysis and natural U blank contributions. In addition, the Elemental Scientific U_{nat} solution was used.

Conventional TIMS source

For the TRU resin loads, the relative deviation (RD) from the measured $n(^{235}U)/n(^{238}U)$ to the certified values of the CRM standards is less than the sum of the uncertainty of the certified ratio[12] and the expanded uncertainty of the measured $n(^{235}U)/n(^{238}U)$ mean (the former being negligible) (Table S1 and Figure 3). Consequently, mass bias cannot be resolved and is not corrected for. In support thereof, analyses of U measured in solution by Modified Total Evaporation-TIMS[14] or bound to resin beads[10] yield mass bias less than 0.15% on $n(^{235}U)/n(^{238}U)$, which is less than our present precision. However, for U_{nat} bound to the anion resin (AG 1-X8) and the cation resin (AG 50W-X12), the relative deviation (RD) from the measured $n(^{235}U)/n(^{238}U)$ to the certified standard values is about 1 to 2 %, which is larger than the expanded uncertainty on these ratios (0.1 to 0.3 %, Table S1 and Figure 3). This calls for external mass bias correction.[12,14]

This positive bias could indicate that both AG 1-X8 and AG 50W-X12 resins induce fractionation or, most likely, that the U_{nat} standard is fractionated. The analysis of U_{nat} on an AG 1-X8 resin bead on the cavity source does not confirm nor invalidate this observation within uncertainty (Table S1). However, the analysis of IRMM-187 bound to an AG 1-X8 resin does not show any positive fractionation (Table S1), hinting toward a fractionation during the commercial preparation of U_{nat}. This observation deserves further investigation, and the analysis of more reference materials on the AG 1-X8 and AG 50W-X12 resins. In Table S1, the accuracy is expressed as the difference between the measured value and a reference value, divided by the latter. Assuming that U_{nat} fractionation is not of instrumental origin, for U_{nat} loads, the reference is chosen as the value of U_{nat} measured for AG 1–X8 (*i.e* 0.00735), whereas for certified standard loads, the references are certified values.[12] In Table S2, $n(^{234}U/^{238}U)$ ratios of the U_{nat} loads are corrected for mass bias internally, on a per integration basis, using the measured $n(^{235}U/^{238}U)$ ratios and CRM 112A as a reference.[12]

The accuracy on $n(^{234}U/^{238}U)$ ratios corrected for peak tailing and background (all protocols) and for mass bias (U_{nat} on anionic and cationic resins) improves by an order of magnitude compared to that of measured $n(^{234}U/^{238}U)$ ratios and ranges from 0.01 to 0.7 %, or 2.5% for the TRU - AquaDag - Re protocol, for which we have seen that the counting statistics was limited by the moderate ionization efficiency (Table S2 and Figure 3). The RD is better than the external precision (2RSD) for all loading protocols (Table S2).

Cavity source

For all TRU and anionic resin loads, the relative deviations RD from the measured $n(^{235}U)/n(^{238}U)$ to the certified values of the CRM standards or to U_{nat} measured for AG 1–X8 on the conventional source (*i.e* 0.00735, Table S1) is of the order of the expanded uncertainty on the measured $n(^{235}U)/n(^{238}U)$ means (Table S1) and do not require mass bias correction. IRMM-187 measured $n(^{235}U)/n(^{238}U)$ shows a negative bias relative to the certified reference, which can be ascribed to a natural U contamination. After a blank correction of 1 pg natural U, as inferred from the analysis of U500, $n(^{235}U)/n(^{238}U)$ is accurate within uncertainty (Table S1).

The relative deviation (RD) from the measured $n(^{234}U)/n(^{238}U)$ to the certified standard values is larger than the expanded uncertainty on the measured $n(^{234}U)/n(^{238}U)$ mean and systematically positive for natural U CRM 112A and U_{nat} loads (5.8 to 8.3%, Table S2).

Considering that the $n(^{234}U)/n(^{238}U)$ ratios lie in the range of $n(^{234}U)/n(^{238}U)$ ratios uncorrected for background by conventional source TIMS (Figure 3), these positive biases are consistent with unaccounted for peak tailing and organic interferences. For non-natural standards that are not blank corrected (IRMM-187 and U500), RD is limited to 0.1 to 1%, owing to smaller peak tailing contributions, in line with their enrichment in ^{234}U compared to natural U (Table S2).

For IRMM-187 blank corrected data, the accuracy remains better than the expanded uncertainty and limited to 0.5%, yielding an accurate $n(^{234}U)/n(^{238}U)$ ratio within uncertainty (Table S2).

Prospects on improving precision and accuracy with the ETH cavity source design

$n(^{235}U)/n(^{238}U)$ ratios on natural reference standards in the 100 to 150 pg range can be measured to expanded uncertainties in the several permil range, external precision in the % range (2RSD) and accuracies within 0.4-0.9%. $n(^{234}U)/n(^{238}U)$ ratios are determined to expanded uncertainties of 0.4 to 2.7 % and an external precision of 5.6 % (2RSD).

The uncertainty is dominated by signal instability, such that a more thermally stable EB assembly would benefit to the precision on U isotope ratios.

These results were acquired with a 0.3 mm wide source slit and, hence, not exploiting the full potential of the cavity source in terms of transmission efficiency. The use of a wider source defining slit would enable data acquisition at higher signal intensities and better counting statistics with simultaneous collection of ^{235}U and ^{238}U masses on Faraday cups. This would require that the associated degradation of the mass spectrum peak shapes is overcome.

The amplifier noise could be improved further by the use of high-resistivity amplifiers.[12,14]

With more precise data, it will be possible to correct for mass bias, whenever applicable, using external correction for $^{235}U/^{238}U$ and internal correction for $^{234}U/^{238}U$ ratios.[12,14] The monitoring of U minor isotope backgrounds, and the peak-tailing and organic interference corrections could also be performed on a per integration basis.[12,14]

Based on counting statistics and detector noise considerations, these combined improvements would significantly improve analytical repeatability and accuracy by a factor 10, down to the permil to sub-permil levels for U sub-ng samples.

CONCLUSIONS

Building on these preliminary results and developing further the instrumental design, the ETH cavity source holds promise

for the development of highly competitive cavity source instruments. Future applications could range from environmental nuclear safeguards and nuclear forensics to space return missions, inclusions in meteorites and deep Earth materials.

ASSOCIATED CONTENT

Supporting Information

PDF including ETH cavity source prototype design main features, a comparison of the outcome of our experiments on the ETH cavity source prototype with Sofie and SIMION simulations and Tables S1 and S2.

AUTHOR INFORMATION

Corresponding Author

* Email : anne.trinquier@ifremer.fr

Present Address

†IFREMER, Département Ressources Physiques et Ecosystèmes de fond de Mer (REM), Plouzané, France.

ACKNOWLEDGMENT

The authors are indebted to U. Menet (ETH) for machining the cavities and D. Niederer (ETH) for his repeated assistance with electronics. H. Bars, M. Finke, A. Nouraout, C. L'Héraut, and M. Dozert (Thermo Fisher Scientific) are thanked for technical support. The authors acknowledge the reviewers and the editor for constructive reviews that improved the quality of the manuscript. AT would like to thank J.F. Wotzlau, A. von Quadt, H. Busemann, R. Wieler (ETH) and L. Sangely (IAEA) for fruitful discussions. This study was performed as part of the ETH Zurich-Commissariat à l'Energie Atomique et aux Energies Alternatives collaboration agreement 188-C-SACO-Av2 and with the support of ETH internal funds. Financial support was also provided by the NCCR PlanetS Technology Platform grant PlanetS-TP-2015-SF2.

REFERENCES

(1) Beyer, G.J.; Herrmann, E.; Piotrowski, A.; Raiko, V.J.; Tyrroff, H. A New Method for Rare-Earth Isotope Separation. *Nucl. Instrum. Methods* **1971**, 96, 437–439.

(2) Johnson, P.G.; Bolson, A.; Henderson, C.M. A High Temperature Ion Source for Isotope Separators. *Nucl. Instrum. Methods* **1973**, 106, 83–87.

(3) Kirchner, R. On the Thermoionization in Hot Cavities. *Nucl. Instrum. Methods Phys. Res A* **1990**, 292, 203–208.

(4) Duan, Y.; Danen, R.E.; Yan, X.; Steiner, R.; Cuadrado, J.; Wayne, D.; Majidi, V.; Olivares, J.A. Characterization of an Improved Thermal Ionization Cavity Source for Mass Spectrometry. *J. Am. Soc. Mass Spectrom.* **1999**, 10, 1008–1015.

(5) Wayne, D.M.; Hang, W.; McDaniel, D.K.; Fields, R.E.; Rios, E.; Majidi, V. The Thermal Ionization Cavity (TIC) Source: Elucidation of Possible Mechanisms for Enhanced Ionization Efficiency. *Int. J. Mass Spectrom.* **2002**, 216, 41–57.

(6) Riciputi, L.R.; Ingeneri, K.B.; Hedberg, P.M.L. Enhanced Ionization Efficiency Using the High Efficiency Cavity Source Implemented on a Magnetic Sector TIMS. *Conference Proceeding IAEA-CN-98/25P* **2003**, 347-353.

(7) Bürger, S.; Riciputi, L.R.; Bostick, D.A.; Turgeon, S.; McBay, E.H.; Lavell, M. Isotope Ratio Analysis of Actinides, Fission Products, and Geolocators by High-efficiency Multi-collector Thermal Ionization Mass Spectrometry. *Int. J. Mass Spectrom.***2009**, 286, 70–82.

(8) Zhai, L.H.; Deng, H.; Wei, G.Y.; Li, Z.M.; Wang, C.H.; Li, X.S.; Zhou, G.Q.; Su, Y.Y., Zhang, Z.B. A New, Ohmic-heating Based Thermal Ionization Cavity Source for Mass Spectrometry *Int. J. Mass Spectrom.* **2011**, 305, 45-49.

(9) Edwards, R.L.; Chen, J.H.; Wasserburg, G.J. ^{238}U-^{234}U-^{230}Th-^{232}Th Systematics and the Precise Measurement of Time over the Past 500,000 Years. *Earth Planet. Sci. Lett.* **1987**, 81, 175-192.

(10) Smith, D.H.; Carter, J.A. A Simple Method to Enhance Thermal Emission of Metal Ions. *Int. J. Mass Spectrom. Ion Phys.* **1981**, 40, 211–215.

(11) Watrous, M.G.; Delmore, J.E.; Stone, M.L. Porous Ion Emitters-A New Type of Thermal Ion Emitter. *Int. J. Mass Spectrom.* **2010**, 296, 21-24.

(12) Richter S.; Kühn, H.; Aregbe, Y.; Hedberg, M.; Horta-Domenech, J.; Mayer, K.; Zuleger, E.; Bürger, S.; Boulyga, S.; Köpf, A.; Poths, J.; Mathew, K. Improvements in Routine Uranium Isotope Ratio Measurements Using the Modified Total Evaporation Method for Multi-collector Thermal Ionization Mass Spectrometry. *J. Anal. At. Spectrom*. **2011**, 26, 550-564.

(13) Trinquier, A. Fractionation of Oxygen Isotopes by Thermal Ionization Mass Spectrometry Inferred from Simultaneous Measurement of ^{17}O/^{16}O and ^{18}O/^{16}O Ratios and Implications for the ^{182}Hf–^{182}W Systematics. *Anal. Chem.* **2016**, 88 (11) 5600–5604.

(14) Trinquier, A.; Komander, P. Precise and Accurate Uranium Isotope Analysis by Modified Total Evaporation Using 10^{13} Ohm Current Amplifiers. *J. Radioanal. Nucl. Chem*. **2016**, 307 (3) 1927-1932.

(15) von Quadt, A.; Wotzlaw, J.-F.; Buret, Y.; Large, S. J. E.; Peytcheva, I.; Trinquier, A. High-precision Zircon U/Pb Geochronology by ID-TIMS Using New 10^{13} Ohm Resistors. *J. Anal. At. Spectrom*. **2016**, 31, 658-665.

(16) Langmuir, I.; Kingdon, K. H. Thermionic Effects Caused by Vapours of Alkali Metals. *Proc. Roy. Soc.* (London) **1925**, A107, 61-79.

(17) Zandberg, E.Y.; Tontegode, A.Y. Some Thermal Emission Properties of Polycrystalline Rhenium Wires. *Sov. Phys. Tech. Phys.* **1965**, 10, 260.

(18) Smith, D.H. Mass Spectrometric Investigation of Surface Ionization. X. Desorption of Uranium Ions and Neutrals from Carburized Rhenium. *J. Chem. Phys* **1971**, 55 (8) 4152-4154.

(19) Coste, A.; Avril, R.; Blancard, P.; Chatelet, J.; Lambert, D.; Legre, J.; Liberman, S.; Pinard, J. New Spectroscopic Data on High-lying Excited Levels of Atomic Uranium. *J. Opt. Soc. Am.* **1982**, 72 103–109.

(20) Waldek, A.; Erdmann, N.; Grüning, C.; Huber, G.; Kunz, P.; Kratz, J. V.; Lassen, J.; Passler, G.; Trautmann, N. RIMS Measurements for the Determination of the First Ionization Potential of the Actinides Actinium up to Einsteinium. *AIP Conf. Proc.* **2001**, 584, 219–224.

(21) Kirchner, R. Progress in Ion Source Development for On-line Seaparators. *Nucl. Instrum. Methods* **1981**, 186, 275-293.

(22) Maden, C.; Baur, H.; Fauré, A.-L.; Hubert, A.; Pointurier, F.; Bourdon, B. Determination of Ionization Efficiencies of Thermal Ionization Cavity Sources by Numerical Simulation of Charged Particle Trajectories Including Space Charge. *Int. J. of Mass Spectrom*. **2016**, 405, 39–49.

(23) Maden, C.; Trinquier, A.; Fauré, A.-L.; Hubert, A.; Pointurier, F.; Rickli, J.; Bourdon, B. Design of a Prototype Thermal Ionization Cavity Source Intended for Isotope Ratio Analysis. *Int. J. of Mass Spectrom*. **2018**, 434, 70-80.

(24) Smith, D.H.; Christie, W.H.; Eby, R.E. The Resin Bead as a Thermal Ion Source: A SIMS Study. *Int. J. Mass Spectrom. Ion Phys.* **1980**, 36, 301–316.

(25) Rokop, D.J.; Perrin, R.E.; Knobeloch, G.W.; Armijo, V.M.; Shields, W.R. Thermal Ionization Mass Spectrometry of Uranium with Electrodeposition as a Loading Technique. *Anal. Chem.* **1982**, 54, 957–960.

(26) Trinquier, A.; Isnard, H.; Aubert, M.; Komander, P. Precise and Accurate U Isotope Analysis using 1E13 Ohm Resistor Amplifiers on a Thermo Scientific ™ TRITON Plus™ MC-TIMS. *Conference Proceeding ESARDA-LC-NA-27342-EN-N* **2015**, 896-901.

(27) Storms, E.K. Sublimation Thermodynamics of UO_{2-x}. *J. Nucl.Mater.* **1985**, 132, 231-243.

(28) Li, X.Q.D.; Radojicic, T.; Vanselow, R. C on Platinum: Work Function Changes Caused by Atomic Carbon and by Two-dimensional Graphite Islands. *Surf. Sci. Lett.* **1990**, 225, L29-L32.
(29) Boulyga, S.F.; Koepf, A.; Konegger-Kappel, S.; Macsik, Z.; Stadelmann, G. Uranium Isotope Analysis by MC-ICP-MS in Sub-ng Sized Samples. *J. Anal. At. Spectrom.* **2016**, 31, 2272-2284.
(30) Ranebo, Y.; Hedberg, P.M.L.; Whitehouse, M.J.; Ingeneri, K.; Littmann, S. Improved Isotopic SIMS Measurements of Uranium Particles for Nuclear Safeguard Purposes. *J. Anal. At. Spectrom.* **2009**, 24, 277-287.
(31) Sharp, N.; Fassett, J.D.; Simons, D.S. Uranium Ion Yields from Monodisperse Uranium Oxide Particles. *J. Vac. Sci. Technol., B.* **2016**, 34 (3), 03H115.
(32) Herrmann, A.; Schumacher, E.; Wöste, L. Preparation and Photoionization Potentials of Molecules of Sodium, Potassium, and Mixed Atoms. *J. Chem.Phys.* **1978**, 68 (5), 2327-2336.

For Table of Contents Only